Coordination Chemistry Reviews, 111 (1991) 1–14
Elsevier Science Publishers B.V., Amsterdam

Repetitive Vibronic Structure Patterns and the Energy Gap in the Spectra of Metal Complexes Caused by Excited State Distortions

Jeffrey I. Zink and Christian Reber

Department of Chemistry and Biochemistry, University of California, Los Angeles, California 90024-1569, USA

Abstract

Two unusual features in the electronic spectra of transition metal compounds which result from excited state distortions are the subject of this paper. The first feature, repetitive patterns of vibronic structure, are interpreted in terms of beats in the time domain between the time-dependent overlaps of two or more modes. The patterns which appear in the emission and absorption spectra of bis(maleonitriledithiolato)palladium are analyzed. The second feature, large gaps separating the emission and absorption spectra of some metal complexes, is a consequence of displacements in two or more normal modes, one of which is not totally symmetric. The active asymmetric b_{1g} mode of $PtCl_4^{2-}$ is modeled by a double minimum potential surface. The electronic spectra and the energy gap are calculated by using the split operator technique for numerical integration of the time-dependent Schrödinger equation.

1. INTRODUCTION

Transition metal compounds are especially interesting for studies of excited state distortions because many modes are displaced and the displacements are frequently large [1]. As a consequence, electronic emission and absorption spectra show interesting features which are not found in the spectra of molecules with a small number of small displacements. Most commonly, the features result from distortions along totally symmetric normal modes. However, in some cases displacements occur along non-totally symmetric modes resulting in molecules which have different point groups in the excited state from that of the ground state.

One striking freature which has been observed is a repetitive pattern in the vibronic structure of the emission spectrum in which a group of bands appears again and again along the band. One of the best examples is observed in the emission spectrum of ruthenocene [2]. A second striking feature which has been observed is the "energy gap", a region betweeen the emission and absorption bands where the intensities of the vibronic structure is vanishingly small. A good example of the energy gap is observed in the spectra of the $PtCl_4^{2-}$ ion [3].

In this paper repetitive patterns of vibronic structure and the energy gap are explained and quantitatively analyzed. Repetitive patterns are shown to result from "beats" in the time-dependent overlap in the time domain. The energy gap is shown to result from distortions along non-totally symmetric normal coordinates. The spectra are calculated by using new methods of numerically integrating the time-dependent Schrödinger equation.

2. THEORY

The time-dependent theory of electronic spectroscopy [4-6] provides a powerful method of both calculating and interpreting the emission and absorption spectra, especially when non-

0010-8545/91/$04.90 © 1991 Elsevier Science Publishers B.V. All rights reserved.

harmonic potential surfaces are involved. Because the theory has been discussed in detail previously,[1-6] only a brief discussion of the general aspects will be given here.

The spectra are governed by the motion of a wavepacket on the multidimensional potential surfaces. The initial wavepacket, $\phi=\phi(t=0)$, is projected onto the potential surface corresponding to the final state (the excited electronic state for an absorption spectrum or the ground electronic state for an emission spectrum). The final surface is in general either displaced relative to the initial surface along normal vibrational coordinates or has a different functional form from that of the intial surface. The wavepacket is in general not an eigenfunction of the final surface and develops in time according to the time-dependent Schrödinger equation. The absorption spectrum is given by [4-6]

$$I(\omega) = C\,\omega \int_{-\infty}^{+\infty} \exp(i\omega t)\,\{\langle\phi|\phi(t)\rangle\ \exp(-\Gamma^2 t^2 + \frac{iE_0}{\hbar}\ t)\}\,dt \qquad (1)$$

where C is a constant and $I(\omega)$ is the absorption cross section. The quantity $\langle\phi|\phi(t)\rangle$ is the overlap of the initial wavepacket, $\phi=\phi(t=0)$ with the time-dependent wavepacket $\phi(t)$. Γ is a phenomenological Gaussian damping factor and E_0 the energy of the origin of the electronic transition. The emission spectrum is given by a similar expression

$$I(\omega) = C\,\omega^3 \int_{-\infty}^{+\infty} \exp(i\omega t)\{\langle\phi|\phi(t)\rangle\ \exp(-\Gamma^2 t^2 + \frac{iE_0}{\hbar}\ t)\}\,dt \qquad (2)$$

where $I(\omega)$ is the intensity in photons per unit volume per unit time at the frequency of the emitted radiation ω.

If it is assumed that (a) the force constants are the same in both ground and the excited states, (b) the potential surfaces are harmonic, (c) the transition dipole moment, μ, is constant and (d) the normal coordinates are not mixed in the excited state, then the overlap $\langle\phi\,|\,\phi(t)\rangle$ has the simple form

$$\langle\phi_k|\phi_k(t)\rangle = \exp\{-\frac{\Delta_k^2}{2}\ (1 - \exp(-i\omega t)) - \frac{i\omega_k t}{2}\} \qquad (3)$$

where ω_k and Δ_k are respectively the vibrational frequency in cm^{-1} and the displacement of the kth normal mode. None of the above assumptions is a requirement of the time-dependent theory. Assumption (a) introduces at most an error of 10 % if the distortions are very large. When the vibrational frequencies in the excited state are not known, this assumption must be used but does not introduce serious error. The harmonic approximation is used because the number of parameters is reduced. If there is no distinct evidence of normal mode mixing, the fits can be done without including the additional parameters of mode mixing.

In most transition metal and organometallic compounds, many modes are displaced. In the case of many displaced normal modes, the total overlap is

$$\langle\phi|\phi(t)\rangle = \prod_k \langle\phi_k|\phi_k(t)\rangle \exp(-iE_0\,t - \Gamma^2 t^2) \qquad (4)$$

where E_0 is the difference in the electronic energy between the minima of the two surfaces and Γ is a damping factor. Thus, the complete overlap is

$$\langle\phi_k|\phi_k(t)\rangle = \exp\{\sum_k\ [-\frac{\Delta_k^2}{2}\ (1 - \exp(-i\omega_k t)) - \frac{i\omega_k t}{2}] - iE_0 t - \Gamma^2 t^2\} \qquad (5)$$

In cases where the simplifying approximations discussed above cannot be used, the time-dependence of the wavepacket evolving on a potential surface can be numerically determined by using the split operator technique of Feit and Fleck [7]. The time dependent Schrödinger equation in two coordinates x and y is

$$i\frac{\partial\phi}{\partial t} = -\frac{1}{2M}\nabla^2\phi + V(x,y)\phi \tag{6}$$

where $\nabla^2 = \delta^2/\delta x^2 + \delta^2/\delta y^2$ and V(x,y) is the potential energy surface. The wavefunction at a time $t + \Delta t$ is [7]

$$\phi(t+\Delta t) = \exp\left(\left(\frac{i\Delta t}{4M}\right)\nabla^2\right)\exp(-i\,\Delta t\,V)\;\exp\left(\left(\frac{i\Delta t}{4M}\right)\nabla^2\right)\phi(x,y,t=0) + O[(\Delta t)^3] \tag{7}$$

The dominant error term is third order in Δt. The initial wavefunction $\phi(x,y,t)$ at t=0 is known. It normally is the lowest energy eigenfunction of the initial state of the spectroscopic transition. The value of the wavefunction at incremental time intervals Δt is calculated by using equation 7 for each point in the (x,y) grid. The autocorrelation function is then calculated at each time interval and the resulting $\langle\phi|\phi(t)\rangle$ is Fourier transformed according to equation 1 or 2 to give the absorption or emission spectrum, respectively.

For the time dependent wavefunctions, the eigenfunctions Ψ_i can be computed [7,8].

$$\Psi_i(x,y,E_i) = \int_0^T \phi(x,y,t)\; w(t)\; \exp\left(\frac{i\,E_i}{\hbar}\,t\right) dt \tag{8}$$

where T is the time encompassed by the calculation, w(t) is a Hanning window function, and E_i is the eigenvalue corresponding to Ψ_i.

The two most important choices which must be made in the numerical calculations are the size of the time steps and the size of the computational grid. The smaller the increment in the time steps and the smaller the spacing between the grid points the greater the accuracy in the calculation. General criteria for initial choices have been published [7,9]. In the work reported here, the time increment is considered small enough and the total time large enough when the plot of the calculated spectrum does not distinguishably change when the increment is halved and the total time is doubled. A time increment Δt=2 fs is usually suitable. The grid spacing is considered to be small enough when the plot of the calculated spectrum does not distinguishably change when the increment is halved. A grid of 256 points/Å is generally suitable for the spectra calculated in this paper.

3. REPETITIVE PATTERNS IN THE SPECTRA OF BIS(MALEONITRILEDITHIOLATE)PALLADATE

The absorption spectrum in the visible region contains two bands, a weak band at 15,700 cm-1 (ε = 64 $M^{-1}cm^{-1}$) and an intense band at 21,770 cm^{-1} (ε=5700 $M^{-1}cm^{-1}$) [10]. The focus in this section is on the vibronic structure in the lowest energy band. Between room temperature and T = 10 K the intensity of the 15700 cm^{-1} band in the single crystal spectrum decreases by a factor of about 8 and the band maximum is blue shifted by about 200 cm^{-1}. At low temperatures, fine structure at the red side of the band can be resolved, as shown in Figure 1. The lines forming the fine structure have half-widths of about 7 cm^{-1}. The very weak origin at 14670 cm^{-1} is followed by a sharp and relatively intense peak 16 cm^{-1} at higher energy. The spectrum exhibits a 150 cm^{-1} progression with an additional 16 cm^{-1} progression

superimposed on it. Between the intense line of highest energy in each group of lines and the adjacent peak of the neighboring series of low intensity lines there is a separation of 28 cm^{-1}.

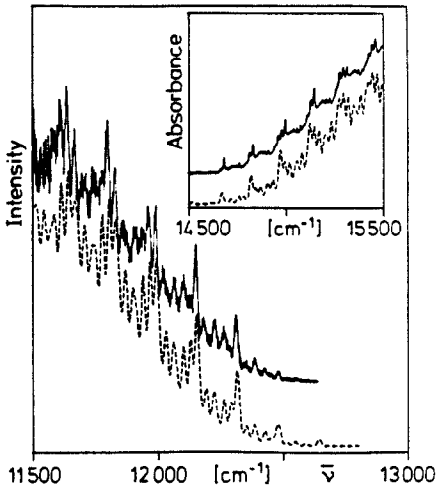

Figure 1. Experimental (solid line) and calculated (dashed line) emission spectra of $((C_2H_5)_4N)_2[Pd(MNT)_2]$. The insert shows the experimental (solid line) and calculated (dashed line) low energy absorption band. The calculated absorption spectrum was obtained by using the same distortions as those for emission.

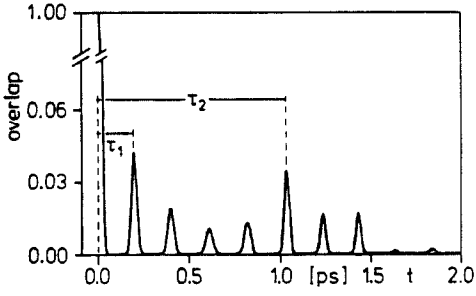

Figure 2. Time dependence of the magnitude of the overlap. Note the two distinct times t_1 (0.2 ps) and t_2 (1 ps) which respectively correspond to the 162 cm^{-1} separation between the most prominent bands and the 26 cm^{-1} separation for the smaller side bands.

The emission spectrum at $T \sim 3$ K shown in Figure 1 shows fine structure similar to that found in the low energy absorption. The two progressions, however, have slightly higher energies, 26 and 160 cm^{-1}, respectively. A conspicuous result is the large energy gap of 2190 cm^{-1} between the absorption peak of lowest energy (14670 cm^{-1}) and the emission peak of highest energy (12480 cm^{-1}). With increasing temperature the emission acquires intensity, but the fine structure disappears.

3.1 Assignment of the Excited Electronic States

The assignment of the optical transitions is based on the following energy order of the one-electron levels: b_{2g} (d_{xy})<a_g (d_z2) < b_{3g}(d_{yz}) <b_{1u} (L_π) <a_g ($d_x2_{-y}2$) <b_{2g} ($L_\pi + d_{xy}$) <b_{1g}(d_{xy}) <a_u,b_{3g} (L_π*). The b_{2g}-MO (with dominant ligand-character) forms the HOMO and the LUMO transforms as b_{1g} (with d_{xy} metal-character).

The weak absorption at 15700 cm^{-1} is assigned to the vibronic transition $^1A_g \rightarrow {}^1B_{3g}$, due to the symmetry forbidden $b_{2g} \rightarrow b_{1g}$ excitation. By vibronic coupling of the states $^1B_{3g}$ and $^1B_{2u}$ this transition acquires oscillator strength.

The emission is due to the electronic transition $^3B_{3g} \rightarrow {}^1A_g$, which is both spin and symmetry forbidden. The corresponding absorption process is too weak to be detectable. The

emission acquires intensity by spin-orbit and vibronic coupling of the state $^3B_{3g}$ with excited singlets. The vibronic character of the emission and of the low-energy absorption manifests itself by (i) the large energy gap (2190 cm^{-1}) between the absorption and emission and (ii) the enhancement of the extinction (absorption) and the intensity (emission) with increasing temperature.

3.2 Calculation of the Fine Structure in the Emission and Absorption Spectra

The intensities and energies of the vibronic bands in the emission spectrum are calculated by using a set of values Δ_k, ω_k, Γ and E_0 by use of equations 1 through 4. E_0 and Γ are determined from the experimental spectrum. In the calculations discussed below the value of E_0 was chosen to be 12642 cm^{-1}, one quantum of the 162 cm^{-1} mode higher in energy than the first clearly discernible peak at 12480 cm^{-1}. Careful inspection of the experimental spectrum reveals weak but nonzero intensity between 12700 cm^{-1} and 12500 cm^{-1}. The best fit to the line widths was obtained by using a value of Γ of 5.5 cm^{-1}. The values of the ω_k's were obtained from the IR and Raman spectra with the exception of the 52 cm^{-1} mode for which no vibrational spectroscopic counterpart is known. This value was obtained from the emission spectrum. The values of the Δ_k's were varied until the best fit between the calculated and experimental spectra was obtained.

The calculated and experimental emission spectra are shown in Figure 1. The agreement between the two is excellent. Because all of the intensity and energy information in the emission spectrum was used, the uncertainties in the values of the parameters are small.

The largest distortion (31% of the sum of all of the Δ_k's) occurs along the 162 cm^{-1} mode. This mode forms the dominant progression in the spectrum. All of the other distortions are smaller by about an order of magnitude. The dimensionless distortions cannot readily be converted to bond length and bond angle changes in units of Å and degrees, respectively, because no normal coordinate analysis of the molecule is available. The 162 cm^{-1} mode is not a simple metal-sulfur stretch [11]. Thus the emitting $^3B_{3g}$ state is distorted along both the Pd-S bond lengths and the S-Pd-S bond angles in the excited state. Because the emission spectrum does not show any evidence of high energy intraligand modes, the distortions within the ligand itself are small and its structure is very similar to that in the ground state.

The low energy absorption band has fine structure which is very similar to that of the emission spectrum. It was therefore tempting to calculate the absorption spectrum by using the distortions obtained form the emission spectrum fit. All of the parameters were left unchanged with the exception of one vibrational frequency, that of the 162 cm^{-1} mode, and E_0. The vibrational frequency in the excited electronic state was decreased to 150 cm^{-1}, the value obtained from the absorption spectrum. E_0 was 14,520 cm^{-1}.

The experimental and calculated absorption spectra are compared in the insert to Figure 1. The agreement in the low energy region is good. These findings support the assignments of the two lowest electronic excited states made in the preceeding section; both $^3B_{3g}$ (the emitting state) and $^1B_{3g}$ derive from the same orbital configuration and therefore are expected to have similar potential energy surfaces and show similar fine structure in the electronic spectra as is observed. The overall band width is poorly reproduced, suggesting that more than one excited state is involved in the absorption band. Thus, the calculations of the vibronic structure provide insight into both the fine structure and the assignments of the lowest energy excited states.

3.3 Analysis of the Repetitive Spacings

The small energy differences between many of the vibronic features in the emission spectrum are exactly equal to the frequency differences between higher energy molecular vibrational modes. The time-dependent theoretical point of view provides a simple interpretation of the small spacings [2]. The new insight arises from interpreting the system in the time domain. In the time domain, the overlap $\langle\phi|\phi(t)\rangle$ as a function of time for a given mode oscillates. The separation between the recurrences is a vibrational period. The total

overlap is the product of the overlaps of each of the individual normal modes. Because each contributing mode has a different vibrational period, the product will be modulated and contain "beats". For two waves, the beat frequency is the difference between the frequencies of the waves.

The modulation of the overlap in the time domain can be clearly seen in Figure 2. This plot shows the overlap which gives the spectrum in Figure 1. The modulation which gives rise to the 26 cm^{-1} separation will be emphasized in this discussion. At t = 0 the total overlap is 1. The plot of the overlap versus time shows the initial falloff and subsequent recurrence at time t_1 = 0.2 ps. The 162 cm^{-1} spacing in the frequency domain is equal to $2\pi/t_1$. Most importantly, the magnitude of the overlap on successive recurrences rises and falls, i.e. the overlap is modulated. In Figure 2, the first maximum of the modulation occurs at the fifth recurrence, i.e., at t = 1 ps labeled t_2. The 26 cm^{-1} spacing in the emission spectrum in Figure 1 corresponds to $2\pi/t_2$ in the time domain and is the difference in the frequencies of the 162 cm^{-1} and the 188 cm^{-1} modes. In this case, the separation between the bands within a cluster is the difference in wavenumbers between the two most highly displaced modes in the excited electronic state.

The damping factor Γ in the time dependent picture ties together the three extremes which can be observed in electronic spectra. If Γ is much larger than the highest frequency, recurrences in the overlap will be totally damped out and the spectrum will consist of a broad unstructured band. If Γ is larger than the difference in the frequencies, the modulation will be damped out but the first recurrence is still observed. The corresponding spectrum will show vibronic structure with the MIME frequency (c.f. section 4.3) [12-14]. If Γ is less than the difference between the two frequencies, successive recurrences are not damped out and a modulation will appear in the overlap. The Fourier transform of the overlap in the time domain is a repeating pattern of bands. The separation between the bands is the difference in frequencies.

4. THE ENERGY GAP RESULTING FROM A DOUBLE MINIMUM POTENTIAL

In the following two sections we calculate the absorption and emission spectra involving a double minimum excited state potential surface which represents a distorted non-totally symmetric normal mode. Many different double minium potential surfaces are used in the literature [15-17]. We chose the function proposed by Coon et. al [17]. A double minimum potential is constructed by superimposing a harmonic potential and a Gaussian barrier:

$$V(Q) = \frac{1}{2} k_{eff} Q^2 + A \exp(-a^2 Q^2) \qquad (9)$$

where k_{eff}, the force constant corresponding to the harmonic term, is calculated as $k_{eff} = 4\pi^2 m(\hbar\omega)^2$ from the vibrational energy $\hbar\omega$ and the reduced mass m of the mode along configurational coordinate Q. The height and width of the Gaussian barrier are determined by the values of A and a respectively.

4.1 Absorption Spectroscopy.

In the absorption process, the wavepacket is transferred vertically from the ground state potential surface to the excited state potential surface. The initial wavepacket in the calculations to be discussed below is the product of a harmonic oscillator ground state eigenfunction times a constant transition moment. This wavepacket is placed on the top of the barrier of the double minimum excited state surface as shown in Figure 3. It is not an eigenfunction of this surface and develops with time according to the time-dependent Schrödinger equation. The magnitude of the wavepacket at several key times is shown in Figure 4. At t=0, the wavepacket is a Gaussian. At short times the wavepacket bifurcates and the two pieces move away from the initial position. In addition, the wavepacket develops a

complicated structure. At t=67 fs the pieces of the wavepacket have reached the outer walls of the double minimum potential and begin to move back to the origin. The much distorted wavepacket returns to its initial position at about t=100 fs then moves away from the barrier again as illustrated at t=116 fs and t=133 fs.

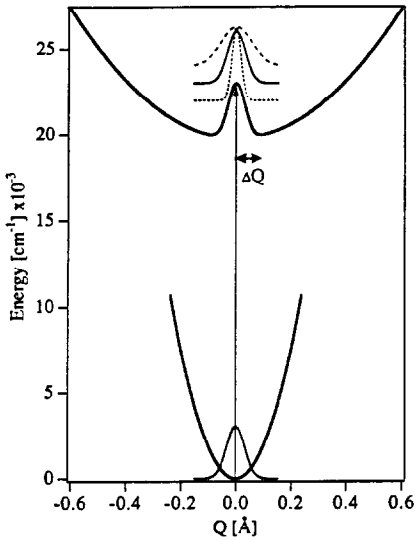

Figure 3. Absorption transition from a harmonic ground state into a double minimum excited state potential. The wavepackets on the excited state surface have $\hbar\omega$ = 300 cm^{-1} (long dashes), 900 cm^{-1} (solid line) and 3200 cm^{-1} (short dashes). The resulting absorption spectra are shown in Figure 6.

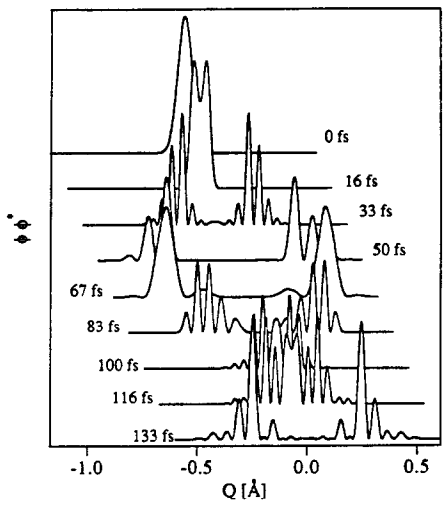

Figure 4. Wavepacket dynamics in the double minimum excited state potential shown in Figure 3. The time dependence of the initial wavepacket with $\hbar\omega$=900 cm^{-1} (solid line, Figure 3) is shown.

The time dependence of the absolute overlap $|\langle\phi|\phi(t)\rangle|$ is shown in Figure 5. The absorption spectrum, given by the Fourier transform of $\langle\phi|\phi(t)\rangle$, is shown in Figure 6 for all three initial wavepackets in Figure 3. The most important features in the spectrum can be understood from the coarse features in the overlap. The overlap is equal to 1 at t=0. At short times, the overlap rapidly decreases as the bifurcated wavepacket moves away from its initial position. The width of the absorption spectrum is related to this initial decrease in overlap; if there were a simple, smooth decrease, the faster the decrease in overlap the broader the spectrum. At longer times the overlap increases to reach a maximum at about t=100 fs. This recurrence in the overlap is related to the vibronic structure in the spectrum. If it were the only recurrence, the spacing in the frequency domain would be equal to c^{-1}(t recurrence)$^{-1}$ corresponding to 330 cm^{-1}.

The trends in the intensity distributions can be explained in terms of the time dependences of the overlaps shown in Figure 5. In all cases, the initial wavepacket ϕ is placed on the top of the barrier. The overlap for a narrow wavepacket, with most of its probability on the part of

the potential surface where the slope is small, decreases slowly with time, and the spectrum has most of its intensity around the energy of the barrier. In contrast, the decrease in part of $\langle\phi|\phi(t)\rangle$ for a broad wavepacket will be faster in time, but part decreases very slowly because a broad wavepacket has appreciable probability on the part of the potential where the slope is steep as well as in the three regions of the potential surface where the slope is small. The result is a complicated spectrum. This behavior is illustrated in the inset of Figure 5: the overlap for the narrow wavepacket ($\hbar\omega$=3200 cm^{-1}, dashed line) decreases slower than that for the broad wavepacket ($\hbar\omega$=300 cm^{-1}, solid line).

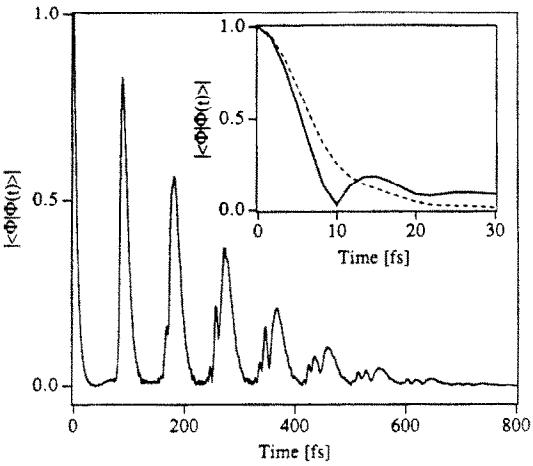

Figure 5. Absolute overlap as a function of time calculated from the wavefunctions shown in Figure 4. Main Figure: absolute overlap $|\langle\phi|\phi(t)\rangle|$ for the wavepacket with $\hbar\omega$=900 cm^{-1}. Inset: overlap at short times for the wavepackets with $\hbar\omega$ = 300 cm^{-1} (solid line) and 3200 cm^{-1} (dashed line).

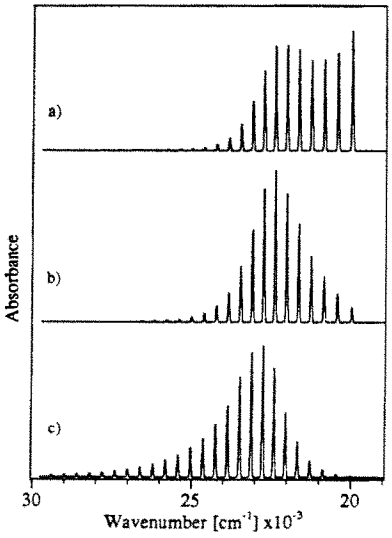

Figure 6. Calculated absorption spectra for the potentials shown in Figure 3. Vibrational frequency of the initial wavepacket is: a) $\hbar\omega$ = 300 cm^{-1}, b) $\hbar\omega$ = 900 cm^{-1}, c) $\hbar\omega$ = 3200 cm^{-1}.

The three spectra shown in Figure 6 illustrate the intensity distributions. They are calculated from the motion of the three wavepackets shown in Figure 3 on the double minimum potential. The only difference between the three calculations is the width of the initial wavepacket. The spectrum in Figure 6a is calculated for a transition from a harmonic ground state with a vibrational frequency of 300 cm^{-1} to the double minimum potential. The initial wavepacket is broad relative to the width of the barrier as illustrated in Figure 3. The spectrum has large intensities in the vibronic bands corresponding to the eigenvalues at the bottom of the excited state minima. In fact, the most intense peak is the lowest energy peak in the spectrum corresponding to the E_0 transition. The intensity of the vibronic features decreases toward higher energy in the absorption spectrum up to the fourth peak and then again increases for the peaks near the energy of the top of the barrier. In this example, the

eighth peak (corresponding to the first vibrational state at the top of the barrier) is not the most intense. The intensity of the peaks corresponding to vibrational levels above the top of the barrier decreases rapidly. The intensity distribution shown in this spectrum results from placing a broad initial wavefunction on the barrier.

The spectrum in Figure 6b is calculated for a transition from a harmonic ground state with a vibrational frequency of 900 cm^{-1}. The initial wavepacket is narrower than that of the preceeding example and the intensities are correspondingly greater in the energy region of the top of the barrier. In this case, the two highest intensity vibronic peaks in the absorption spectrum are those corresponding to the levels immediately below and above the barrier, respectively. The intensity of the E_0 peak is dramatically reduced from that in Figure 6a. The overall intensity distribution accidentally appears to be similar to a Poisson distribution.

The bottom spectrum is calculated for a transition from a ground state with a frequency of 3200 cm^{-1}. The initial wavepacket is narrow relative to the width of the barrier and the largest intensity is found in the vibronic band corresponding to the energy level at the top of the barrier. The intensities of the vibronic bands from states near the bottom of the minima are low. In fact, the E_0 band and the next two peaks to higher energy are barely observed in the spectrum. Much more of the intensity in the spectrum is found in the peaks corresponding to energy levels well above the top of the barrier.

The origin of the apparent Energy Gap between experimental absorption and emission spectra is related to the width of the initial wavepacket relative to that of the excited state potential barrier. The spectrum in Figure 6c illustrates a specific example in which an energy gap might be observed. The E_0 peak and the peak next to it are less than 2% of the intensity of the biggest peak in the spectrum. In an experimental spectrum such weak transitions might be buried in the noise and might not be observable. The intensities of the low energy peaks in a spectrum depend sensitively on both the specific potential surface and the initial wavepacket and can be significantly smaller than those in the examples described here. The specific case of the potential surface and initial wavepacket for $[PtCl_4]^{2-}$ is discussed later.

4.2 Emission Spectroscopy.

In the emission process, the wavepacket is transferred vertically from the excited state potential surface to the ground state potential surface as shown in Figure 7. In the spectra to be discussed below, the excited state potential surface is the same double minimum surface that was used in the calculations of the absorption spectra. Thus the initial wavepacket is a vibrational eigenfunction of the double minimum surface times the transition moment. The vibrational eigenfunctions of the excited state surface are calculated by using equation 8. The two lowest energy eigenfunctions are shown in Figure 7.

The energy separation between the lowest pair of levels is 0.4 cm^{-1} for the double minimum potential surface used here. The next higher pair of levels are 455 cm^{-1} above the lowest pair. Thus the emission spectrum is the sum of the spectra calculated by using the two lowest energy eigenfunctions as initial wavepackets. The thermal weighting for the two lowest levels is about equal at T = 10 K. The 0.4 cm^{-1} separation between the two spectra which are added is not discernable in the spectrum that is calculated with a damping factor of 15 cm^{-1} because the line widths are larger than the level splitting by an order of magnitude. The two lobes of the gerade (or ungerade) wavefunction can be physically visualized as moving toward each other, crossing each other, and coming to rest on opposite sides of the potential in half a vibrational period. The resulting spectrum will show a spacing of twice the vibrational frequency. However, the ungerade function has non-zero overlap only with the ungerade functions of the ground electronic state and only the odd quantum number bands have intensity in the spectrum. The gerade function has non-zero overlap only with the gerade functions of the ground electronic state and only the even quantum number bands have intensity in the spectrum. Both individual spectra are shown in Figure 8 and in the total spectrum both the even and the odd quantum number bands are observed.

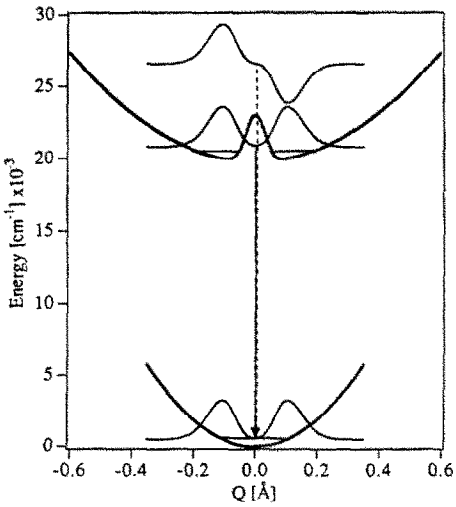

Figure 7. Emission transition from a double minimum excited state potential into a harmonic ground state potential. The lowest vibrational levels of the excited state coincide on the energy scale of the Figure; their eigenfunctions are offset for clarity. Both functions were propagated on the ground state surface to obtain the emission spectra in Figure 8.

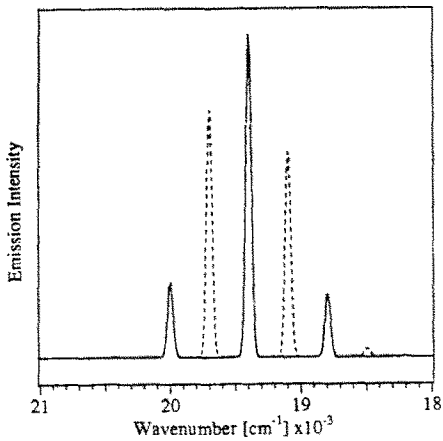

Figure 8. Calculated emission spectra. The solid spectrum is obtained by propagating the lowest excited state eigenfunction only (solid arrow in Figure 7), the dashed spectrum is obtained by propagating the next higher eigenfunction (dashed arrow in Figure 7).

The physical meaning of relaxed emission (originating from the lowest level(s) of a double minimum potential surface) is that the moleculer geometry is distorted from that of the ground state. The point group of the emitting molecule is different from that of the molecule in the ground state. The new point group contains all of the symmetry elements which the two states have in common. The coordinate of the double minimum potential is totally symmetric in this new point group. In the example discussed above, the probability is greatest of finding the molecule with a bond length change of ±0.09 Å along the non-totally symmetric coordinate as shown by the eigenfunctions in Figure 7. If the coordinate is the b_{1g} coordinate of a square planar molecule as will be discussed for the spectra of $K_2[PtCl_4]$, the distorted molecule will be a rhombus (D_{2h}).

4.3 Energy Gap in the Spectra of $K_2[PtCl_4]$

The absorption and emission spectra of $K_2[PtCl_4]$ contain two unusual features. First, a large (≈1800 cm^{-1}) region between the onset of the emission and absorption bands is found in which no absorbance or emission is experimentally observed. (Most commonly, the emission and absorption spectra overlap at the electronic origin transition (E_0).) Careful studies with thick crystals have shown that this "energy gap" is not simply a consequence of a spin-forbidden absorption band which is weak in comparison to nearby bands and which was overlooked in the absorption spectrum [3,18]. Theoretical work has shown that all the spin- and parity-forbidden transitions in $PtCl_4^{2-}$ should gain considerable intensity via spin-orbit coupling [19]. In addition, analysis of the vibronic progression in the emission spectrum has shown that the energy gap is not simply a consequence of a large distortion along totally

symmetric modes giving rise to very small intensities in the vibronic bands near the origin [3]. The second unusual feature is the spacing between the vibronic bands in the emission spectrum. The bands are regularly spaced, but the energy between the bands does not correspond to any normal vibrational mode of the molecule in the crystal[3]. This absence of a normal mode of the required frequency, the missing mode effect (MIME), has been recognized and analyzed in other molecules [12-14]. It is a consequence of two or more displaced normal modes.

The two-dimensional ground and excited state potential surfaces which quantitatively describe the unusual spectroscopic features are shown in Figure 9. The two normal coordinates are the totally symmetric Pt-Cl stretching normal mode (a_{1g}) and the non-totally symmetric in-plane Pt-Cl stretching mode (b_{1g}). In the ground electronic state, the two coordinates are described by uncoupled harmonic oscillator potentials

$$V(a_{1g}, b_{1g}) = \frac{1}{2} k_{a1g} Q_{a1g}^2 + \frac{1}{2} k_{b1g} Q_{b1g}^2 - E_{zp} \qquad (10)$$

k_{a1g} and k_{b1g} are the force constants for the a_{1g} and b_{1g} modes, respectively. They are calculated from the experimental vibrational energies of 329 cm^{-1} (a_{1g}) and 304 cm^{-1} (b_{1g}).[3] In the excited electronic state the a_{1g} mode is described by a harmonic potential and the b_{1g} mode by the double minimum potential discussed in the previous section. This surface is given by:

$$V(a_{1g}, b_{1g}) = \frac{1}{2} k_{a1g} (Q_{a1g} - \Delta Q_{a1g})^2 + \frac{1}{2} k_{eff} Q_{b1g}^2 + A \exp(-a^2 Q_{b1g}^2) - E_{zp} \qquad (11)$$

The global minima of this surface correspond to a molecule in which the bonds are elongated along the totally symmetric coordinate relative to those in the ground electronic state, i.e. the surface is displaced along the totally symmetric normal coordinate. The ridge or barrier (where $Q_{b1g}=0$ and $\partial V/\partial Q_{b1g}=0$) in the double minimum potential along the nontotally symmetric b_{1g} coordinate is not displaced relative to the minimum in the ground state potential as is required by symmetry. Of course the minima of the double minimum potential are displaced relative to the minimum of the ground state potential by a distortion ΔQ.

The absorption spectrum is calculated by vertically transferring the lowest energy two-dimensional ground state eigenfunction to the excited state potential surface as shown by the arrow denoted A in Figure 9. The wavepacket thus experiences a non-zero slope in the a_{1g} dimension but is on the top of the barrier in the b_{1g} dimension as discussed in the previous section. The emission spectrum is calculated in a similar manner. In this case the two lowest energy eigenfunctions of the excited state potential surface first have to be calculated because the energy separation between them is less than 1 cm^{-1}. They are calculated by using equation 8 . These eigenfunctions are than vertically transferred to the ground state potential surface as shown by the vertical arrow pointing down in Figure 9. Both of the two-dimensional wavepackets experience non-zero slopes in both the a_{1g} and b_{1g} dimensions. The time development is calculated by using equation 7 and the spectrum by using equations 1 and 2. Because the two lowest vibrational eigenstates are thermally populated, the spectrum is the thermally weighted sum of the spectra individually calculated from propagating each eigenfunction. The physical meaning of the vertical emission transition is that the molecule has distorted into a rhombus (D_{2h}) in the excited electronic state. Thus the emission spectrum can be thought of as originating from a new molecule with new selection rules. Of primary importance to the platinum spectrum, the vibrational mode which had b_{1g} symmetry in the square planar ground state molecule now has a_{1g} symmetry in the D_{2h} point group.

The emission spectrum and the absorption spectrum are both calculated from the ground and excited state potential surfaces shown in Figure 9 and defined by equations 10 and 11. The ground state potential surface is fully defined by the experimentally determined vibrational frequences. The excited state potential uses the following parameters: $\hbar\omega_{eff}$ = 153 cm^{-1}, m = 35.453 g/mole, A=2980 cm^{-1}, a=12.670 $Å^{-1}$, ΔQ_{a1g} = 0.120 Å and E_0 = 14435 cm^{-1}. The distortion ΔQ along the b_{1g} coordinate is 0.151 Å, calculated from the potential parameters.

The only adjustable parameters in the calculation are the 3 parameters defining the shape of the double minimum potential ($\hbar\omega_{eff}$, a, A) and the parameter defining the displacement of the excited state potential along the a_{1g} coordinate, ΔQ_{a1g}. The values for the damping factor Γ are 87 cm^{-1} and 123 cm^{-1} for the calculated emission and absorption spectrum, respectively.

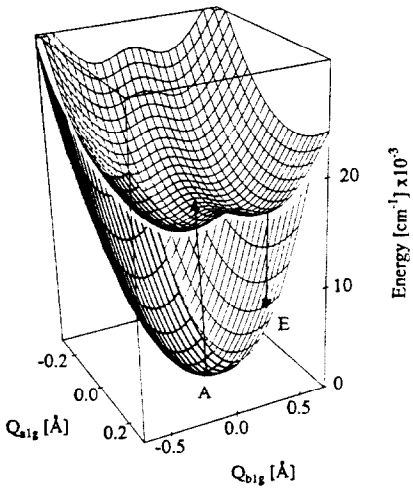

Figure 9. Two dimensional potential surfaces for the ground state and the lowest energy excited state of $K_2[PtCl_4]$. The maxima of the absorption and emission spectra are indicated by the arrows labeled A and E, respectively.

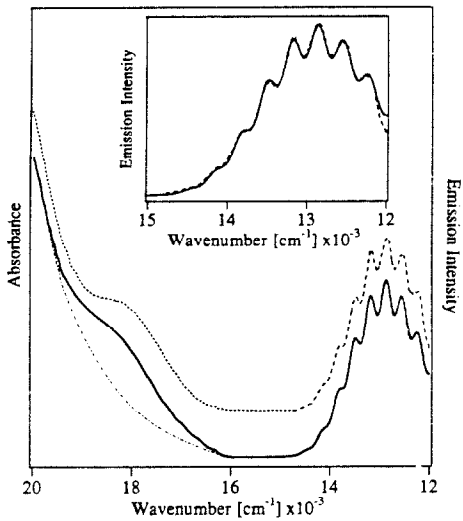

Figure 10. Experimental and calculated emission and absorption spectra of $K_2[PtCl_4]$. Main Figure: experimental emission spectrum (T=10K, long dashes), experimental absorption spectrum (10K, short dashes), calculated spectra (solid lines, offset for clarity). The baseline for the calculated absorption spectrum is interpolated from the high and low energy parts of the experimental data and is a guide for the eye only. The inset shows the experimental (dashed) and calculated (solid) emission spectra in more detail.

The calculated emission and absorption spectrum are compared to the experimental spectra in Figure 10. The details of the experimental spectra including the band width and energy of the absorption band, the band width and energy of the emission band, the energy gap, and the MIME, are accurately calculated.

The energy gap in the spectra of $K_2[PtCl_4]$ is caused by the distortion along the non-totally symmetric normal coordinate. When the initial wavepacket in this dimension is narrow with respect to the width of the barrier, the intensities of vibronic bands near the origin will be very weak relative to those corresponding to energies near the top of the barrier. Thus the

absorption spectrum has extremely small intensity in the region of the energy gap which is not measurable even with relatively thick crystalline samples.

The vibronic structure in the emission spectrum results from motion of the wavepacket in two dimensions. The average spacing in the progression is 315 ±5 cm^{-1}. This spacing does not match that of any normal mode in $K_2[PtCl_4]$ and is an example of the MIME. The requirements for a MIME to be observed are that two or more normal modes must be involved and that the damping factor Γ must be large enough to kill all but the first major recurrence in the total overlap in the time domain. As shown in the inset of Figure 10, the MIME spacing is accurately calculated by using the potential surfaces from Figure 9. The fit of the experimental spectrum is excellent. The MIME in the emission spectrum of $K_2[PtCl_4]$ is thus a new type in which the initial wavepacket is displaced along a totally symmetric mode and in which the two thermally populated components from the global minima of a double minimum potential combine to give a spacing which does not correspond to any of the vibrational frequencies of the ground state potential surface.

The normal coordinate equilibrium displacement in the excited state determined by the fit can readily be expressed in terms of bond length changes in Å. Only the magnitudes are determined. For the d-d transition to the σ antibonding $d_{x^2-y^2}$ orbital it is logical to assume that the a_{1g} displacement corresponds to bond lengthening. The increase in the length of each Pt-Cl bond from the a_{1g} mode is 0.06 Å. In the b_{1g} direction, one pair of chloride ligands opposite to each other elongate by 0.08 Å while the other pair contracts by the same amount. The net result is a rhombic molecule whose bond length changes are shown in Figure 11.

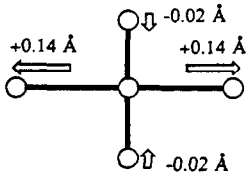

Figure 11. Excited state distortions for $PtCl_4^{2-}$ in $K_2[PtCl_4]$ determined from absorption and emission spectra.

5. SUMMARY

The time-dependent picture of electronic spectroscopy provides both a physical picture and the calculational method for treating unusual spectroscopic features caused by excited state distortions along multiple normal modes. Repetitive patterns of vibronic structure are interpreted and calculated as beats in the time-dependent overlap. The energy gap is caused by distortions along non-totally symmetric normal modes. In order to calculate and analyze both the absorption and emission spectra including the energy gap, a double minimum potential surface and the split operator technique must be used.

6. ACKNOWLEDGEMENTS

This paper is dedicated to the memory of our friend and colleague Prof. Dr. Günter Gliemann. We thank Dr. J. Gauss and Prof. E. J. Heller (University of Washington, Seattle) for their implementation of the wavepacket propagation algorithm. This work was made possible by a grant from the National Science Foundation.

7. REFERENCES

1 J.I. Zink, and K.S. Kim Shin, Molecular Distortions in Excited Electronic States Determined from Electronic and Resonance Raman Spectroscopy, in: Advances in Photochemistry, vol. 16, D.H. Volman, G.S. Hammond, and D.C. Neckers (eds.) John Wiley & Sons, Inc., New York, 1991.
2 G. Hollingsworth, K.S. Shin, and J.I. Zink, Inorg. Chem., 29 (1990) 2501.
3 D.M. Preston, W. Güntner, A. Lechner, G. Gliemann, and J.I. Zink, J. Am. Chem. Soc., 110 (1988) 5628.
4 E.J. Heller, J. Chem. Phys., 68 (1978) 3891.
5 E.J. Heller, J. Chem. Phys., 68 (1978) 2066.
6 E.J. Heller, Acc. Chem. Res., 14 (1981) 368.
7 M.D. Feit, J.A. Fleck, and A. Steiger, J. Comp. Phys., 47 (1982) 412. For an introductory overview see J.J. Tanner, J. Chem. Ed., 67 (1990) 917.
8 Numerical eigenfunctions obtained by eq. 5 agreed with analytical eigenfunctions for harmonic and Morse potentials and also to numerical eigenfunctions for the potential in eq. 7 calculated with a time independent method to at least five digits at each grid point (U. Blukis and J.M. Howell, J.Chem.Ed., 60 (1983) 207).
9 D. Kosloff and R. Kosloff, J. Comp. Phys., 52 (1983) 35.
10 W. Günter, G.Gliemann, H. Kunkely, C. Reber and J.I. Zink, Inorg. Chem., 29 (1990) 5238.
11 R.J.H. Clark and P.C. Turtle, J. Chem. Soc. Dalton Trans. (1977) 2142.
12 L. Tutt, D. Tannor, E.J. Heller, and J.I. Zink, Inorg. Chem., 21 (1982) 3859.
13 L. Tutt, D. Tannor, J.W. Schindler, E.J. Heller, and J.I. Zink, J. Phys. Chem., 87 (1983) 3017 .
14 L.J. Larson and J.I. Zink, Inorg. Chem., 28 (1989) 3519.
15 G. Herzberg, Infrared and Raman Spectra of Polyatomic Molecules Van Nostrand Reinhold, New York, 1945, 220ff.
16 M.F. Manning, J. Chem. Phys., 3 (1935) 136.
17 J.B. Coon, N.W. Naugle, and R.D. McKenzie, J. Mol. Spect., 20 (1966) 107.
18 H.H. Patterson, J.J. Godfrey, and S.M. Khan, Inorg. Chem., 11 (1972) 2872.
19 L.G. Vanquickenborne and A. Ceulemans, Inorg. Chem., 20 (1981) 796.